JOURNAL OF MATERIALS SCIENCE 30 (1995) 883–890

Compositional modification of titanium carbide powders by induction plasma treatment

T. ISHIGAKI*, J. JUREWICZ†, J. TANAKA, Y. MORIYOSHI
National Institute for Research in Inorganic Materials, 1-1, Namiki, Tsukuba-shi, Ibaraki 305, Japan

M. I. BOULOS†
†*Plasma Technology Research Centre(CRTP), Department of Chemical Engineering, University of Sherbrooke, Sherbrooke, Quebec, Canada J1K 2R1*

Non-stoichiometric titanium carbide powders were treated in an r.f. induction plasma. The composition of plasma gas, reactor pressure and powder feed rate were changed as experimental parameters, but plate power was kept constant. As the titanium carbide powders passed through the plasma, they melted, partially evaporated, and finally solidified. During the in-flight process, compositional modification was noted involving lattice modification and a change of the non-stoichiometry of titanium carbide depending on the plasma and powder feeding conditions. These were mostly due to the removal of carbon and oxygen impurity in titanium carbide while melting. The μ-AES analysis indicated that the removal of carbon occurred in the plasma treatment. The deposits formed from the vapour phase consisted mainly of very fine cubic crystals, some tens of nanometres in size, with an appreciable number of vacancies at carbon sites.

1. Introduction

A thermal plasma is characterized by relatively high temperature and the presence of reactive chemical species. Powders injected into a plasma are subjected, in-flight, to modifications of their morphology, chemical composition and crystal structure in a short time (of the order of tens of milliseconds). With growing interest in the processing of powders under plasma conditions, such as in plasma-spray coating, it is becoming increasingly important to know the in-flight interaction between the plasma and the powder particles. The variation in shape, morphology, chemical composition, and crystal structure in plasma-treated powders reflects the history of the powder through the powder processing, and has a strong influence on the properties of the coating. Precise characterization of powders is one of the important tools that can be used to gain an understanding of the basic processes involved in plasma treatment.

Titanium carbide, with a very high melting temperature, ~3290 K [1], has excellent properties, such as high electrical conductivity, high hardness, good corrosion resistance and high-temperature strength [2]. Some composites, such as TiC–Al_2O_3, also show improved toughness [3] and erosion resistance [4]. Titanium carbide is thus a material of considerable interest for plasma-spray coating applications.

The non-stoichiometry of TiC_x can vary over a large range ($0.5 < x < 1$), while its cubic crystal structure, of NaCl-type, remains unchanged [5]. When powders are melted in a thermal plasma, the temperature of the particle surfaces in the plasma is maintained between melting and boiling temperatures. The chemical interaction plays a crucial role under such conditions: at temperatures above 3000 K, the molten titanium carbide particles can react with chemical species, such as hydrogen atoms. The resultant change in chemical composition reflects the interaction with the plasma. Such knowledge is basic in various plasma-processing applications such as reactive spray-coating, which is also of considerable interest [6, 7].

In this work, the in-flight behaviour of titanium carbide powders was studied by examination of plasma-treated powders. Attention was paid to the modification of chemical composition in plasma-treated powders. It is known that the electronic [8, 9] and mechanical ([2] pp. 141–84) properties, the surface energy [10] and ion transport [11] in titanium carbide strongly depend on changes in its non-stoichiometric composition.

2. Experimental procedure

A schematic diagram of the induction plasma torch used in this work is shown in Fig. 1. The plasma was generated using a radiofrequency (r.f.) power supply with a nominal oscillator frequency of 3 MHz and a maximum r.f. power of 50 kW. Three gas streams were introduced into the torch; these are the powder carrier gas, the plasma gas and the sheath gas shown

* Author to whom all correspondence should be addressed.

0022–2461

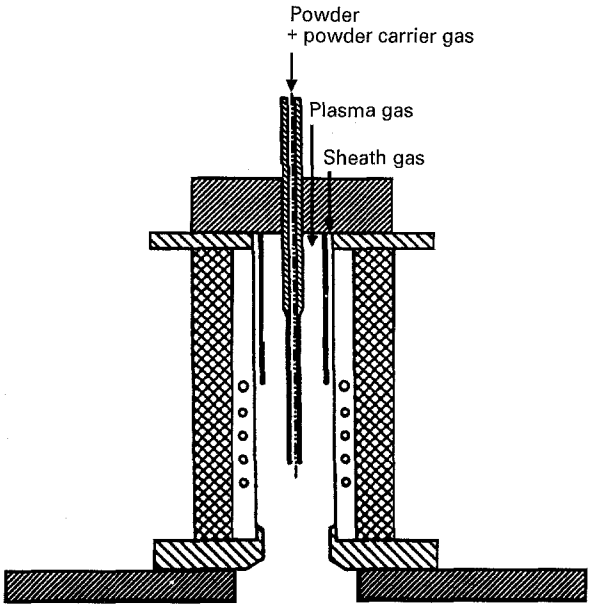

Figure 1 A schematic diagram of the plasma torch.

TABLE I Plasma generating parameters and powder feeding conditions

	(a)	(b)	(c)
Sheath gas (1), Ar ($l\,min^{-1}$)	82	82	82
Sheath gas (2), H_2 ($l\,min^{-1}$)	9.6	2.3	9.6
Plasma gas, Ar ($l\,min^{-1}$)	28	28	28
Powder carrier gas (1), Ar ($l\,min^{-1}$)	6.9	6.9	5.4
Powder carrier gas (2), CH_4 ($l\,min^{-1}$)			1.5
Plate power (kW)		32	
Reactor pressure (kPa)		53–93	
Powder feed rate ($kg\,min^{-1}$)		0.004–0.040	

in the figure. The operating conditions are summarized in Table I. The plasma is confined in a 50 mm inner diameter water-cooled quartz tube. The plasma discharges into a water-cooled stainless steel chamber with an inner diameter of 254 mm and a length of 1020 mm in which the absolute pressure was varied over the range of 53–93 kPa.

Titanium carbide powders were axially injected into the centre of the discharge through a powder-feeding probe with the carrier gas. The powder, supplied by Japan New Metals, TiC-M, shown in Fig. 2a has a particle size of less than 325 mesh (45 μm) and the chemical composition is $TiC_{0.95}$. Oxygen atoms dissolve easily into the titanium carbide lattice [5], and the commercial titanium carbide powders usually contain a small amount of oxygen impurity. The oxygen content of the present powder is 0.26 wt%, which is slightly higher compared to the usual level of 0.1–0.2 wt%, with this particle size. In this work, the powder with higher oxygen content was used in order to study the role of oxygen.

The powders, which passed through the plasma, were collected on the reactor wall, reactor bottom,

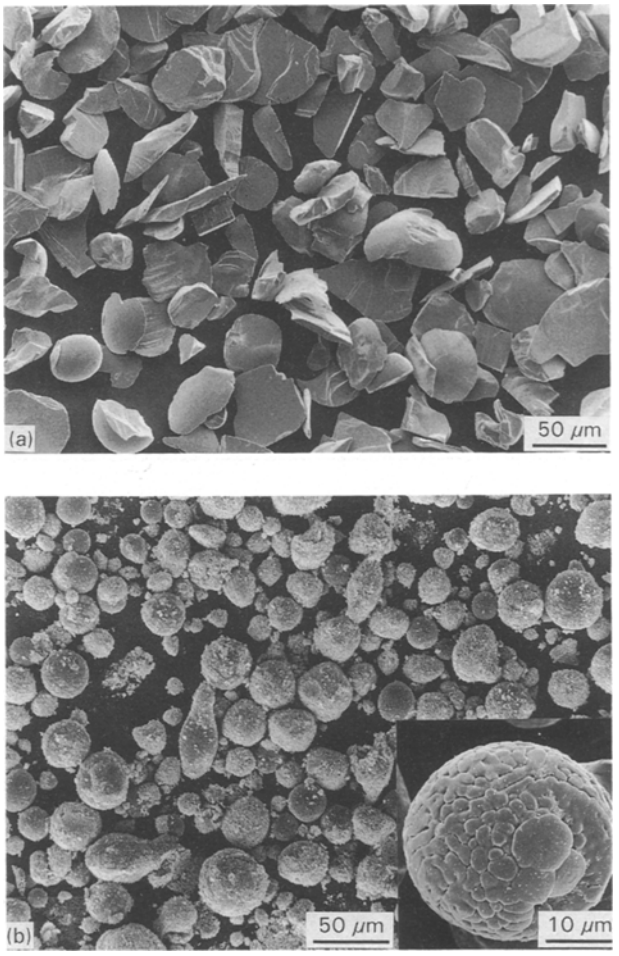

Figure 2 Scanning electron micrographs of (a) the initial titanium carbide powder, and (b) a plasma-treated powder (plasma composition (a) in Table I, reactor pressure 80 kPa, powder feed rate $0.004\,kg\,min^{-1}$).

cyclone and filter. In all experiments, most of the powder was collected on the reactor wall. Preliminary deposition experiments were tried on graphite substrates, which were placed in the reactor chamber, 100 and 150 mm below the end of the plasma torch confining tube.

The morphology of the treated powders was observed with a scanning electron microscope (SEM, Akashi, ISI-DS130). The crystal phase was identified using X-ray diffractometry. For the determination of lattice constant of titanium carbide, silicon (Johnson-Matthey, purity >99.999%) was used as an internal standard. The content of carbon in the initial powder and the plasma-treated powders were determined using a carbon analyser (Horiba, EMIA-511), and the oxygen and nitrogen contents were determined using a LECO, TC-136 instrument.

In order to determine the distribution of constituent atoms, the cross-sections of plasma-treated powders were analysed using scanning Auger electron spectroscopy (μ-AES, VG Microlab 320-D). For analysis the powders were encapsulated in an electroconductive resin and polished with diamond powders on a disc. A 10 kV accelerating voltage of electron beam was applied for excitation. The beam diameter was about 300 nm. Before AES measurement, the surfaces of sectioned particles were sputtered using an argon ion

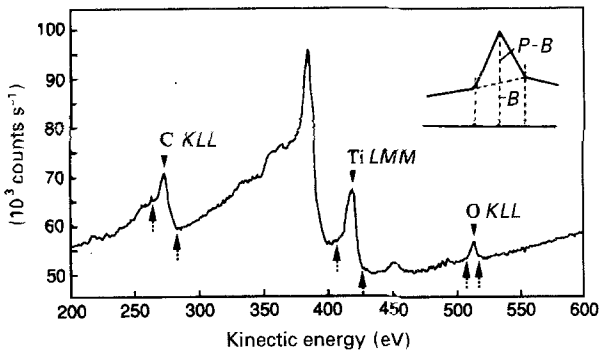

Figure 3 Auger electron spectra detected from the cross-section of a titanium carbide particle. The background intensity was defined to be the average of the intensities of both sides of the signal peak as indicated by arrows.

beam to remove any surface contamination. The distribution of constituent atoms was estimated using the Auger spectra for Ti*LMM*, C*KLL*, and O*KLL* transitions, indicated by arrows in Fig. 3. The relative peak height was defined by $(P\text{-}B)/B$, where P and B are the peak and the background intensities, respectively. The background intensity, B, was defined by the average of the intensities of both sides of the peak (Fig. 3). Typical distributions of relative peak height are given in Fig. 8 (see later).

For transmission electron microscopy (TEM), the powders were dispersed in carbon tetrachloride, placed on copper grids, and observed with a JEOL JEM-2000EX TEM operated at 200 kV.

3. Results and discussion

3.1. Thermodynamics of the plasma treatment

Earlier studies reported by the authors dealt with the in-flight treatment of alumina powders in r.f. induction plasmas [12, 13]. Alumina has rigid stoichiometric composition and a large number of metastable phases. The change in shape and size distribution and the formation of metastable phases in alumina powders varied with the change in heat transfer from the plasma to the particles and particle residence time in the tail-flame region. The change in morphology, such as whisker and ultra-fine particles, and crystal structure of the deposits from the vapour phase were related to the supersaturation in the vapour phase.

In the case of titanium carbide, special attention was paid to the change of its non-stoichiometry. Equilibrium compositions were calculated for the present experimental condition by minimization of the Gibbs free energy [14, 15] in the system composed of argon, hydrogen and non-stoichiometric TiC_x using the SGTE and GTT thermochemical databases [16, 17]. For simplicity, the oxygen impurities in the titanium carbide were excluded. The atomic and molecular species included in the calculation are as follows

(gas phase) Ar, H, H_2, Ti, C, C_2, C_3,

C_4, C_5, CH, CH_2, CH_3,

CH_4, C_2H, C_2H_2, C_2H_4, C_2H_6,

(liquid phase) C–Ti,

(solid solution phase) α-Ti(hcp A3 phase),

β-Ti(bcc A2 phase),

TiC_x(fcc B1 phase),

(solid phase) C(graphite).

For C to C_5, the data by Gustafson [18] were adopted. The melt of C–Ti was treated as the simple substitutional and associated solutions with the Redlich–Kister–Muggianu polynomial [19, 20] yielding the following expression for the Gibbs energy per mole of titanium atoms

$$G_m^{liq} = X_C {}^\circ G_C^{liq} + X_{Ti} {}^\circ G_{Ti}^{liq} + RT(X_C \ln X_C + X_{Ti} \ln X_{Ti}) + X_C X_{Ti}[{}^0L_{Ti,C}^{liq} + {}^1L_{Ti,C}^{liq}(X_C - X_{Ti})] \quad (1)$$

$${}^0L_{Ti,C}^{liq}(\text{J/mol Ti}) = -155000 - 33.3\,T \text{ [21]} \quad (2)$$

$${}^1L_{Ti,C}^{liq}(\text{J/mol Ti}) = -20000 + 9.62\,T \text{ [21]} \quad (3)$$

where X_C and X_{Ti} are the mole fractions, and ${}^\circ G_C^{liq}$ and ${}^\circ G_{Ti}^{liq}$ are the Gibbs energy of liquid carbon and titanium, respectively. $L_{Ti,C}^{liq}$ is the interaction energy between titanium and carbon atoms. The fcc B1 phase was treated using an interstitial sublattice model [22], which gives the Gibbs energy in the following form for (Ti)(C, Va)

$$G_m^{B1} = Y_C {}^\circ G_{Ti:C}^{B1} + Y_{Va} {}^\circ G_{Ti:Va}^{B1} + RT(Y_C \ln Y_C + Y_{Va} \ln Y_{Va}) + Y_C Y_{Va}[{}^0L_{Ti:C,Va}^{B1} + {}^1L_{Ti:C,Va}^{B1}(Y_C - Y_{Va})] \quad (4)$$

$$1 - Y_{Va} = Y_C = \frac{X_C}{1 - X_C} \quad (5)$$

$${}^0L_{Ti:C,Va}^{B1}(\text{J/mol Ti}) = -75800 \text{ [21]} \quad (6)$$

$${}^1L_{Ti:C,Va}^{B1}(\text{J/mol Ti}) = -76000 \text{ [21]} \quad (7)$$

where ${}^\circ G_{Ti:C}^{B1}$ and ${}^\circ G_{Ti:Va}^{B1}$ are the Gibbs energy of states when all of the interstitial sites are filled with carbon atoms and vacancies, respectively, i.e. Ti_1C_1 and Ti_1Va_1. $L_{Ti:C,Va}^{B1}$ is the interaction energy between carbon atoms and vacancies. α-Ti(hcp A3 phase) and β-Ti(bcc A2 phase) were also treated by the interstitial sublattice model in the same way as the fcc B1 phase.

The calculated equilibrium composition given in Fig. 4 shows that liquid TiC appears in the temperature range 3080–3130 K. The Ti–C phase diagram evaluated by Toth [2] is shown in Fig. 5: the melting behaviour of titanium carbide varies depending on its non-stoichiometric composition. The calculated equilibrium carbon contents in the Ti–C melt and the non-stoichiometric TiC_x are also included. It is noted that the increase of temperature leads to the gradual reduction of carbon content in TiC_x up to the melting temperature, beyond which a sudden decrease of the carbon content is observed.

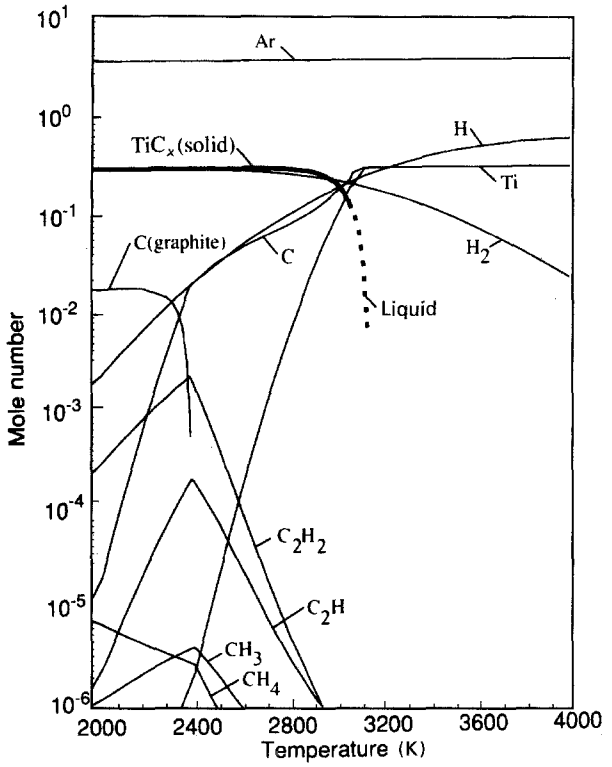

Figure 4 Thermodynamic equilibrium in the Ar–H_2–TiC system (pressure 80 kPa, Ar 3.78 mol, H_2 0.31 mol, $TiC_{0.95}$ 0.3 mol).

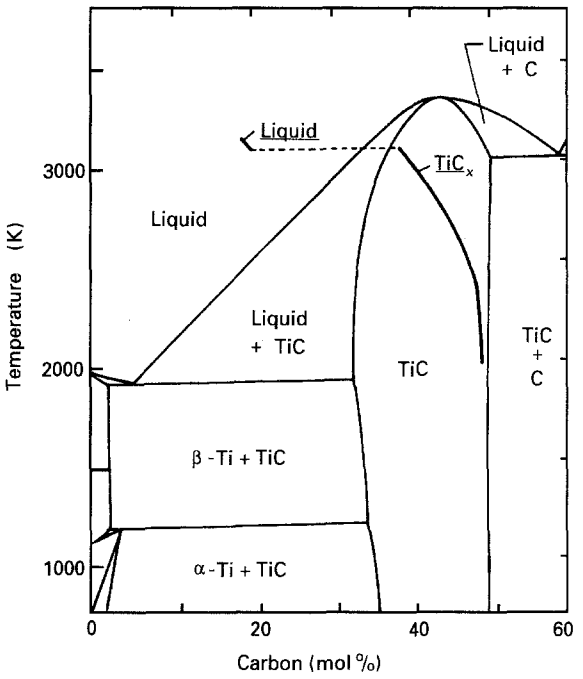

Figure 5 Phase diagram of the Ti–C system [2]. The equilibrium carbon content in the Ti–C melt and the non-stoichiometric TiC_x determined by calculation in Fig. 4 is shown by a thick line.

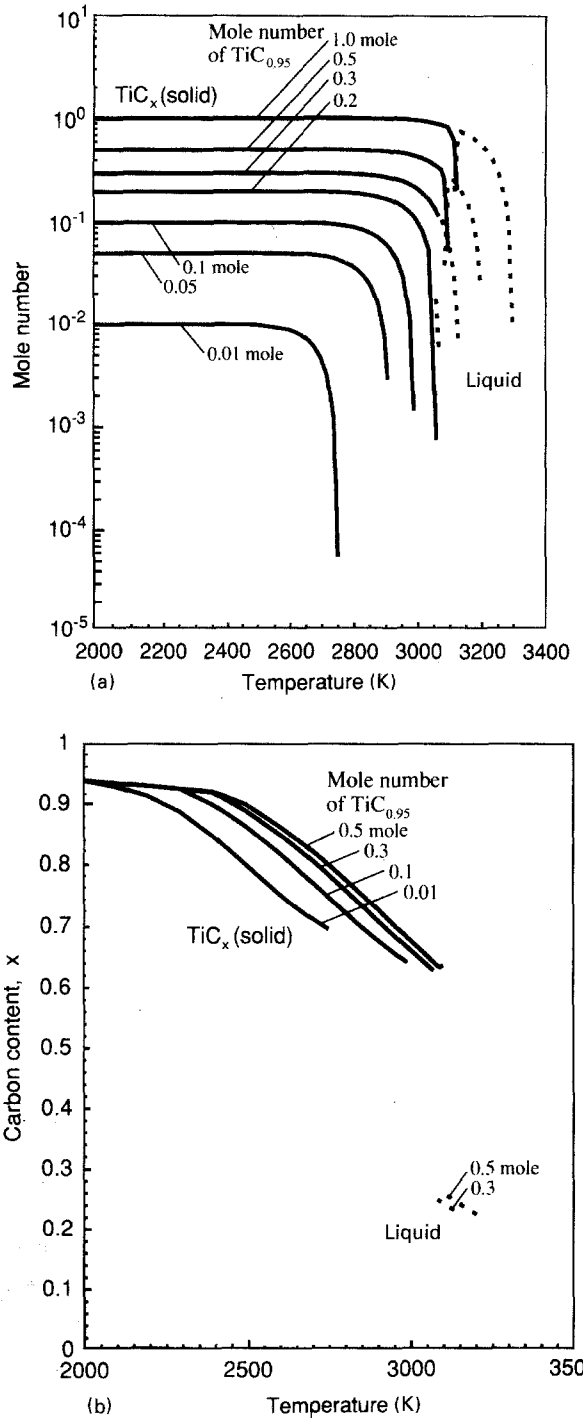

Figure 6 Variation in the melting and evaporation of titanium carbide as a function of the mole fraction of $TiC_{0.95}$ in the Ar–H_2 system (pressure 80 kPa, Ar 3.78 mol, H_2 0.31 mol). (a) Variation in melting and evaporation temperatures. (b) Variation in carbon contents in TiC_x (solid) and Ti–C melt.

In addition to the compositional modification resulting from heating and melting of the powder, the chemical composition also changes through the evaporation and subsequent condensation process. The condition can also be described using the thermodynamic analysis. In Fig. 6, the variation of carbon content is shown as a function of the mole fraction of $TiC_{0.95}$ in the system. The concentration of titanium and carbon, evaporated from the titanium carbide powder is relatively low in the region far enough away from the original powder particles. When consolidation occurs from the vapour phase, the condition corresponds to the small mole fraction of $TiC_{0.95}$ in Fig. 6. Under such conditions, consolidation passes directly from the vapour to the solid phase with a relatively low carbon content in the formed aerosol, giving rise to a high concentration of carbon vacancies in its lattice.

The variation of carbon deficiency induced by the heating, melting and vaporization followed by

deposition from the vapour phase, is responsible for the non-uniformity of the chemical composition in plasma-treated powders.

3.2. Compositional modification in melted particles

Scanning electron micrographs of plasma-treated titanium carbide powder are shown in Fig. 2b. The melting and evaporation of the particles was partially achieved, because the plasma-treated powder consists of spheroidized and partially spheroidized particles, and submicrometre fumes deposited on them. For the same plasma composition and reactor pressure, the number fraction of spheroidized particles decreased with the increase of powder feed rate. These particles were always covered with fumes formed through condensation from the vapour phase. The surface of the spheroidized particle shown on the right-hand side of the figure, in which the fumes were removed by treatment in an ultrasonic bath of ethanol, is smooth, a clear indication that they were molten in the plasma.

X-ray diffractometry showed that no other crystal phase but titanium carbide was formed in the powders collected. Crystalline carbon was not found even in the powders treated with $Ar–H_2–CH_4$ plasma, where the amorphous carbon could be formed from the vapour phase. It is seen in Fig. 7a that the plasma treatment gave rise to an increase in the lattice constant, which changed depending on the plasma generation and powder feeding conditions.

Careful measurement of the lattice constant can be used to detect changes in chemical composition, because it is known that the lattice constant of titanium carbide varies depending on the ratio of carbon and titanium atoms [2]. Also, the dissolution of oxygen lowers the value of the lattice constant [23]. As the amounts of evaporation were rather small, the lattice constant obtained by X-ray diffractometry reflects the average chemical composition in the spheroidized particles. In the estimated chemical composition, $[Ti][C]_x[O]_y$, by the carbon and oxygen analysis, the value of x was more than 0.9, where the lattice constant has a one-to-one relation with composition, TiC_x, as shown in the inset figure of Fig. 7. The reference data for $TiC_{0.95}$, $TiC_{0.94}$ and $TiC_{0.93}$ are indicated in Fig. 7. This change is probably due to the removal of oxygen and/or carbon atoms from their lattice sites.

Plasma generation and powder feeding conditions affected the interaction between plasma and fed particles. At the lower powder feed rate, a particle absorbs more heat and, as seen in Fig. 7, the lattice constant increases with decreasing powder feed rate, irrespective of the plasma generating conditions. Comparing the results for two runs using $Ar–H_2$ plasma at 60 kPa, it is noted that the lattice constant increased with increasing hydrogen content in the plasma. This may be related to the increase in the heat transfer rate from the plasma to the particles. It is known that the thermal conductivity of $Ar–H_2$ plasma increases with increasing hydrogen content, and that the higher thermal conductivity gives rise to higher heat transfer

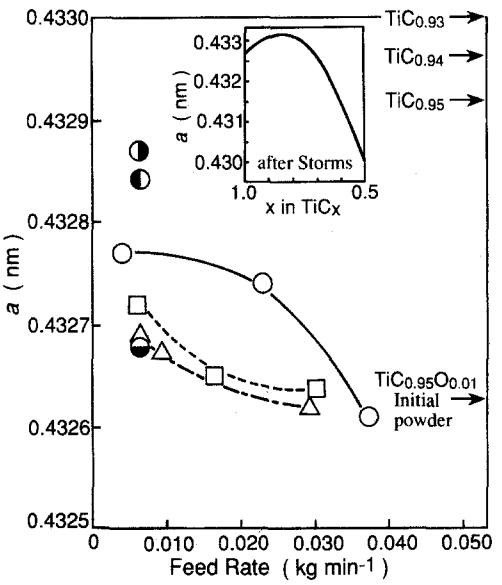

Figure 7 Variation in the lattice constant of titanium carbide induced by plasma treatment: (◑, ◐, ○, ◒) $Ar–H_2$, plasma composition (a); (□) $Ar–H_2$, plasma composition (b); (△) $Ar–H_2–CH_4$, plasma condition (c). (◑) 93 kPa, (◐) 80 kPa, (○, □, △) 67 kPa, (◒) 53 kPa. Reference data [5] is inset of the lattice constant of TiC_x as a function of composition.

rates from the plasma to the particles [24]. The effect of the reactor pressure on the powder treatment was also investigated. The results given in Fig. 7, for an $Ar–H_2$ plasma, show that when the reactor pressure increases from 53 kPa to 93 kPa, the lattice constant increases at the powder feed rate, $\sim 0.006\,kg\,min^{-1}$. This is due to the decrease of the plasma velocity and the corresponding increase of the particle residence time in the plasma with the increase of the reactor pressure. By the addition of methane to the plasma, the removal of carbon/oxygen atoms was suppressed. This may be related to the change in chemical composition of the plasma surrounding titanium carbide particles rather than changes in the thermal conductivity of the plasma, which is hardly affected by such a small concentration of CH_4.

Deposition on a graphite substrate was attempted for the plasma composition (a) at pressures of 67 and 80 kPa, and (b) at 67 kPa, with a powder feed rate of $0.007–0.008\,kg\,min^{-1}$. As mentioned above, heat transfer from the plasma to a particle varies in the following order: (a) at 80 kPa > (b) at 67 kPa > (c) at 67 kPa. Greater heat transfer gives rise to a larger degree of powder melting and deposition. The deposition efficiency was observed to vary in the same order. Higher deposition rates were attained with a substrate 100 mm below the end of the plasma-confining tube compared to that at 150 mm. This is mainly due to cooling of melted particles. The lattice constant of titanium carbide showed no appreciable change between the powders collected on the reactor wall and the deposits on the substrate, regardless of the substrate position.

In order to observe directly plasma-treated powders, μ-AES was employed. Because Auger electron spectroscopy uses the electrons emitted from a solid surface of a few nanometres in depth, it is applicable to

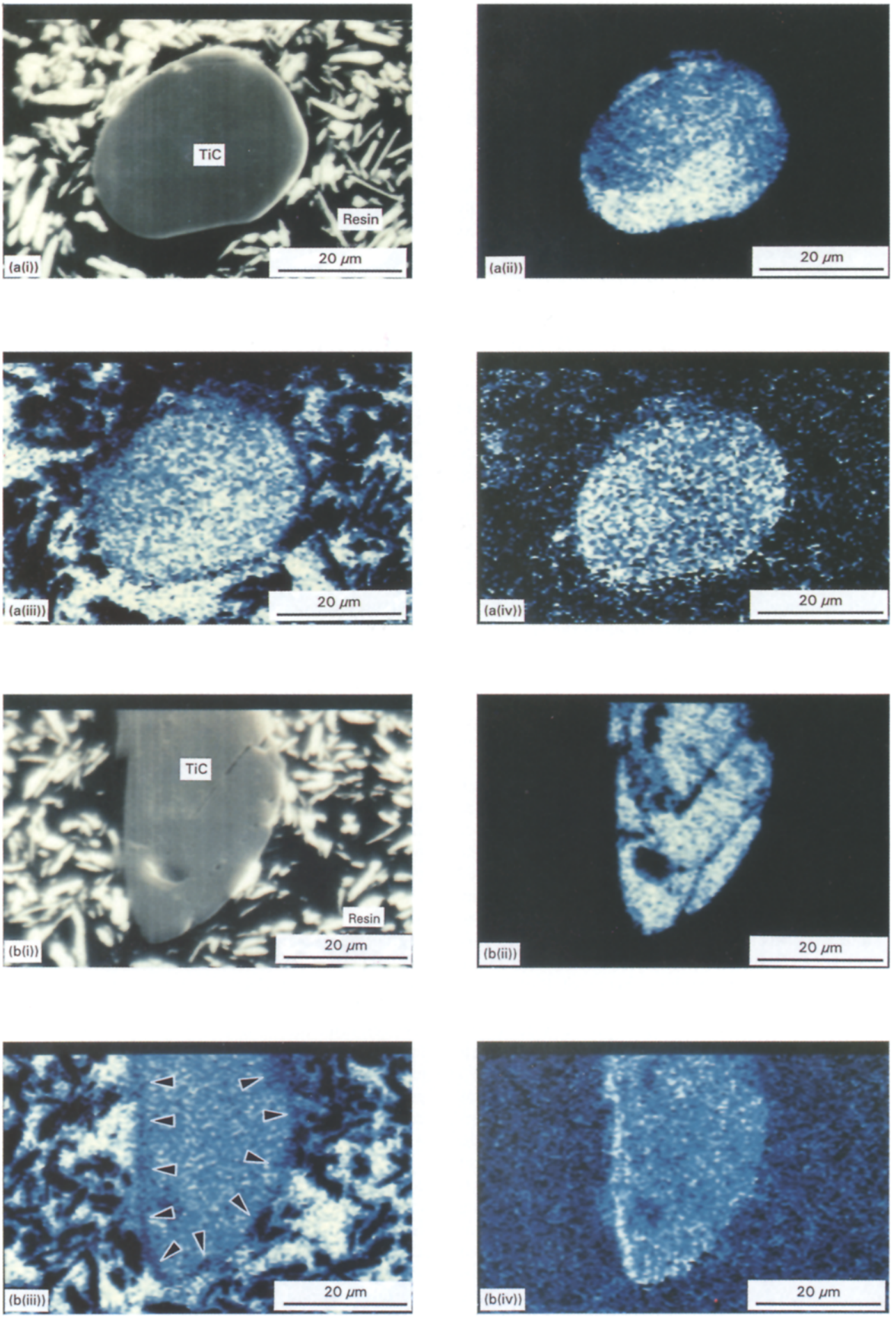

Figure 8 Distribution of elementary atoms in the cross-section of plasma-treated powders (plasma composition (a) in Table I, reactor pressure 80 kPa, powder feed rate 0.004 kg min^{-1}) for (a) a completely melted particle and (b) a partially melted particle, obtained by μ-AES. (i) SEM, (ii) titanium, (iii) carbon, (iv) oxygen.

the estimation of the distribution of elementary atoms in a particle. In Fig. 8a (i) and b (i), scanning electron micrographs of the cross-section of completely and partially melted titanium carbide particles mounted in electroconductive resin are shown, respectively. In Fig. 8a (ii–iv) and b (ii–iv), the bright areas indicate a high intensity of the Auger signal and the dark areas indicate a low intensity.

Under the plasma and powder feeding conditions of Fig. 8, most particles were melted and spheroidized. As can be seen in Fig. 8a (ii–iv), even in the completely melted particle, the distribution of elementary atoms is not uniform. Although titanium carbide itself is brittle, such non-uniformity in the chemical composition in a particle would hinder the propagation of a crack and give high fracture toughness to the particle. Completely melted particles could be polished without the appearance of any cracks, while small cracks were observed to develop in partially melted particles during polishing. This may be related to the homogeneous texture of the particles.

The observation of a partially melted particle provided information for the understanding of the compositional change induced by the plasma treatment. The dark region in the distribution of the Auger signals from titanium atoms (Fig. 8b (ii)), corresponds to the concavities in the cross-section (Fig. 8b (i)). The distribution of titanium atoms in it can be regarded as uniform. However, the signal distribution from carbon atoms has dark contrast at the edge of the particle, as indicated by arrows in Fig. 8b (iii). The thickness of the layer is 1–1.5 μm. The dark layer is certainly an indication of high carbon deficiency along the particle surface. However, it was not clearly confirmed whether the oxygen deficiency was formed by the plasma treatment. The data from μ-AES showed that the oxygen content was high in the surface layers, as shown in Fig. 8b (iv). As the powders were collected and stored in air, oxygen atoms could easily be incorporated into carbon site vacancies of the titanium carbide lattice.

As was suggested by the thermodynamic calculation shown in Fig. 5, the lattice modification during melting is probably due to the removal of carbon atoms in the present plasma treatment, which is accelerated by the chemical reaction. The results of thermodynamic calculation given in Fig. 4 indicate the presence of hydrogen atoms in the temperature range of titanium carbide melting. This suggests that chemical species in the plasma such as CH, CH_2, CH_3, C_2H, C_2H_2 and OH, would be formed by the following reaction with hydrogen atoms

$$TiC_xO_y(l) + \beta H(g) \rightarrow TiC_{x'}O_{y'}(l) + \beta' CH_m(g) + \beta'' OH(g) \quad (8)$$

Also, it could be possible that carbon species are removed from titanium carbide melt as CO, which is very stable in the gas phase even at high temperatures

$$TiC_xO_y(l) \rightarrow TiC_{x'}O_{y'}(l) + \delta CO(g) \quad (9)$$

The preferential removal of oxygen also agrees with the impurity refining during single-crystal growth. Oxygen impurities were not detectable in the grown single crystals, although the feed material had an oxygen impurity of about 0.15 wt% [25]. Although kinetic data are not available for the reaction between the melt and the gas phase, the idea of removal during melting is consistent with the result that no appreciable difference was obtained in the lattice constant in the collected powders on the reactor wall and the deposits on the substrate. The powders in these two cases had the same thermal histories in the high temperature region of the plasma, but had different ones during their solidification steps.

3.3. Formation of carbon site vacancies during the deposition from the vapour phase

The composition of deposits obtained from the vapour phase was also noted to undergo chemical changes. The spongy mass surrounding the spheroidized particles in Fig. 2 is the deposit from the vapour phase. As shown in the transmission electron micrograph given in Fig. 9, the deposit consists of very fine nanocrystalline cubic particles some tens of nanometres in

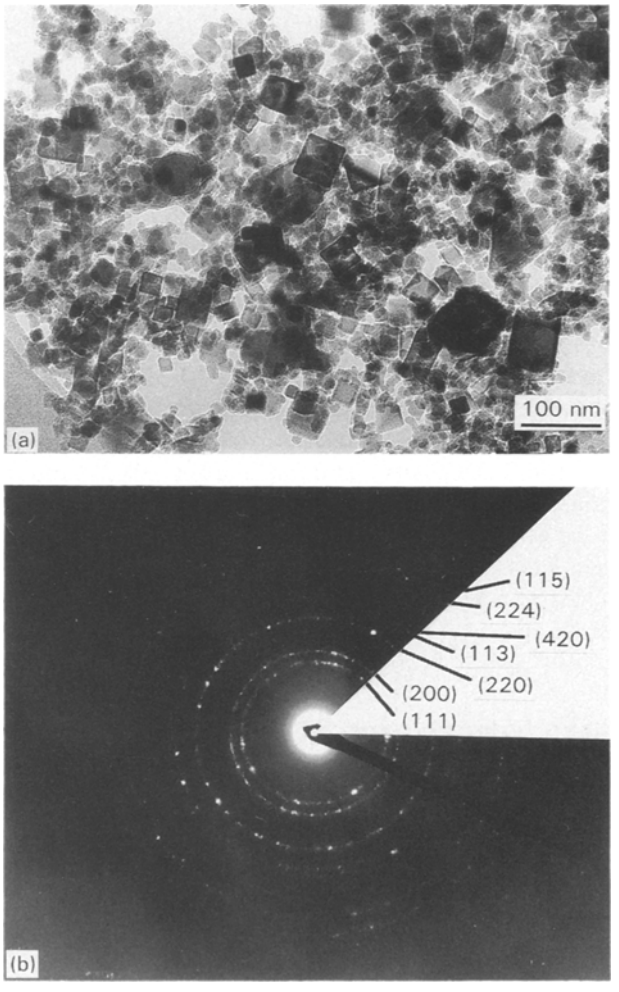

Figure 9 (a) Transmission electron micrograph of the deposits from the vapour phase, and (b) the electron diffraction pattern.

size. The faceted morphology shows that the deposit was not formed by the condensation to liquid droplets which subsequently crystallized, but more likely by the direct condensation from the vapour to the solid phase. The electron diffraction pattern revealed that the particles were composed of TiC with a lattice constant of 0.42–0.43 nm. This small value is an indication of the presence of a high concentration of carbon vacancies and oxygen incorporation in the lattice structure. Based on the lattice data given by Storms [5] for the TiC_x system, the value of x in our case is estimated to be close to 0.5 (see Fig. 7). Such a low carbon content in the lattice structure, further suggests the formation of these nanocrystalline cubic powder through its direct condensation from the vapour to the solid phase as indicated in Fig. 6b. The formation of a high concentration of carbon vacancies was also reported in the synthesis of ultrafine powders of some transition metal carbides. Ultrafine powders of ZrC_{1-x} were formed by d.c. thermal plasma deposition [26]. Phase formation in the Zr–C system is very similar to that of the Ti–C system. By using r.f. induction [27] and d.c. [28] thermal plasmas, ultrafine powders of cubic WC_{1-x} ($0.3 < x < 0.4$) were obtained.

4. Conclusion

Thermal and chemical interactions between the r.f. induction plasma and the immersed powder particles were clarified experimentally. Titanium carbide powders were subjected to modification in their chemical composition and morphology by r.f. thermal plasma treatment. Compositional changes of titanium carbide were observed in the melted and spheroidized powders which seemed to depend strongly on the plasma generation and powder feeding conditions. This reflected changes in the heat transfer from the plasma to the particles and changes in the concentration of the chemical species in the plasma. A mechanism has been proposed for the removal of carbon and oxygen atoms from the titanium carbide lattice. μ-AES observations showed that the plasma treatment gave rise to a non-uniformity in chemical composition of the melted particles. Deposits obtained from the vapour phase were ultrafine nanocrystalline cubic TiC powders. The large number of vacancies observed at carbon sites was attributed to the rapid cooling of the vapour on leaving the high-temperature region of the discharge.

Acknowledgement

The authors thank Mr Y. Kitami, Mr M. Tsutsumi and Mr C. Akita for co-operation in the TEM and SEM observations and the μ-AES measurement, respectively.

References

1. N. W. CHASE Jr, C. A. DAVIES, J. R. DOWNEY Jr, D. J. FRURIP, R. A. McDONALD and A. N. SYVERUD, *J. Phys. Chem. Ref. Data* **14** Suppl. 1 (1985).
2. L.E. TOTH, "Transition Metal Carbides and Nitrides" (Academic Press, New York, London, 1971).
3. W. P. WAHI and B. ILSCHNER, *J. Mater. Sci.* **15** (1980) 875.
4. S. WADA and N. WATANABE, *J. Ceram. Soc. Jpn.* **96** (1988) 327.
5. E. K. STORMS, "The Refractory Carbides" (Academic Press, New York, 1967) pp. 3, 5, 8.
6. P. G. TSANTRIZOS, L. T. MAVROPOULOS, M. I. BOULOS, J. JUREWICZ and K. CHEN, in "Proceedings of the 10th International Symposium on Plasma Chemistry", edited by Ehlemann, H. G. Lergon and K. Wiesemann (Bochum, Germany, 1991) 1.4–2.
7. Z. Z. MUTASIM and R. W. SMITH, *ibid.*, 1.4–10.
8. J. REDINGER, R. EIBLER, P. HERZIG, A. NECKEL, R. PODLOUCKY and E. WIMMER, *J. Phys. Chem. Solids* **46** (1985) 383.
9. S. OTANI, T. TANAKA and Y. ISHIZAWA, *J Mater. Sci.* **21** (1986) 1011.
10. L. RAMQVIST, *Int. J. Powder Met.* **1** (1965) 2.
11. H. J. MATZKE, *Philos. Mag. A* **64** (1991) 1181.
12. T. ISHIGAKI, J. JUREWICZ and M. I. BOULOS, in "Proceedings of the 10th International Symposium on Plasma Chemistry", 1.4–18, edited by Ehlemann, H. G. Lergon and K. Wiesemann (Bochum, Germany, 1991) 1.4–18.
13. T. ISHIGAKI, Y. BANDO, Y. MORIYOSHI and M. I. BOULOS, *J. Mater. Sci.* **28** (1993) 4223.
14. G. ERIKSSON and K. HACK, ChemSage Ver. 2.2 (GTT mbH, Herzogenrath, 1991).
15. *Idem., Metall. Trans.* **21B** (1990) 1013.
16. "SGTE Pure Substance Database", Ver. 1.0, developed by Scientific Group Thermodata Europe (GTT mbH, Herzogenrath, 1991).
17. "GTT Standard Data Files" from "SGTE Solution Database", Ver. 1.0, C-Ti, BIN02300 developed by GTT (GTT mbH, Herzogenrath, 1991).
18. P. GUSTAFSON, *Carbon* **24** (1986) 169.
19. O. REDLICH and A. T. KISTER, *Int. Eng. Chem.* **40** (1948) 345.
20. Y. M. MUGGIANU, M. GAMBIO and J. P. BROS, *J. Chim. Phys. Chim. Biol.* **72** (1975) 83.
21. K. BALASUBRAMANIAN and J. S. KIRKALDY, McMaster University, Hamilton, Ontario, Canada, unpublished work (1989).
22. M. HILERT and L. I. STAFFANSSON, *Acta Chem. Scand.* **24** (1970) 3618.
23. P. P. J. RAMAEKERS and R. METSELAAR, Br. Ceram. Proc. **37** (1986) 119.
24. P. PROULX, J. MOSTAGHIMI and M. I. BOULOS, *Int. J. Heat Mass Transfer* **28** (1985) 1327.
25. S. OTANI, T. TANAKA and Y. ISHIZAWA, *J. Crystal Growth* **83** (1987) 481.
26. Z. P. LU, T. W. OR, L. STACHOWICZ, P. KONG and E. PFENDER, in "Materials Research Society Symposium Proceedings", Vol. 190, edited by D. Aperian and J. Szeckely (MRS, Pittsburgh, 1991) p. 77.
27. T. KAMEYAMA, T. TSUNODA, A. MOTOE, T. UEMATSU and K. FUKUDA, *Funtaioyobi Funmatsuyakin* **38** (1991) 109.
28. P. KONG, M. SUZUKI, R. YOUNG and E. PFENDER, *Plasma Chem. Plasma Process.* **3** (1983) 115.

Received 18 January
and accepted 16 May 1994